Journal of
Marine Science
and Engineering

MDPI

Article

Energy, Exergy and Environmental Analysis of ORC Waste Heat Recovery from Container Ship Exhaust Gases Based on Voyage Cycle

Long Lyu [1,2], Ankang Kan [1,*], Wu Chen [1,*], Yuan Zhang [1] and Bingchun Fu [1]

1 Merchant Marine College, Shanghai Maritime University, Shanghai 201306, China; lyulong@jmi.edu.cn (L.L.); zhangyuan@shmtu.edu.cn (Y.Z.); 202130110116@stu.shmtu.edu.cn (B.F.)
2 School of Marine Intelligent Engineering, Jiangsu Maritime Institute, Nanjing 211147, China
* Correspondence: ankang0537@126.com (A.K.); chenwu@shmtu.edu.cn (W.C.); Tel.: +86-21-38282971 (A.K.); +86-21-38282927 (W.C.)

Abstract: Recovering the waste heat of a marine main engine (M/E) to generate electricity was an environmental way to minimize the carbon dioxide emissions for ships, especially with organic Rankine cycle (ORC) technology. The M/E had variable loads and operating times during voyage cycle, which directly affected the ORC thermodynamic potential. In this paper, a voyage cycle-based waste heat utilization from the M/E was introduced to provide reliable evaluation for proposing and designing ORC. The effect of various M/E loads and operating times on ORC performance among three dry-type substances was analyzed. The environmental impact was presented based on the data from one voyage cycle navigation of objective container ship. The results showed that Cyclohexane was capable of net power while Benzene was more suitable for thermal efficiency. The evaporator and condenser were the main irreversible components of the ORC system and required further optimization. Taking the operational profile into consideration, the evaporation pressures were 922–1248 kPa (Cyclohexane), 932–1235 kPa (Benzene) and 592–769 kPa (Toluene), respectively. During the voyage cycle, the carbon dioxide emissions were 99.68 tons (Cyclohexane), 96.32 tons (Benzene) and 60.99 tons (Toluene), respectively. This study provided certain reference for the design and investigation of ORC application to further improve the energy efficiency for container ship.

Keywords: voyage cycle; waste heat recovery; organic Rankine cycle; working fluid

Citation: Lyu, L.; Kan, A.; Chen, W.; Zhang, Y.; Fu, B. Energy, Exergy and Environmental Analysis of ORC Waste Heat Recovery from Container Ship Exhaust Gases Based on Voyage Cycle. *J. Mar. Sci. Eng.* **2023**, *11*, 2029. https://doi.org/10.3390/jmse11102029

Academic Editor: Leszek Chybowski

Received: 7 October 2023
Revised: 19 October 2023
Accepted: 21 October 2023
Published: 23 October 2023

1. Introduction

The extensive use of fossil fuels had existed as an environmental problem caused by marine vessels. The global warming effect was one of the most frequently stated environmental problems. Several studies data from the International Maritime Organization (IMO) Fourth 2020 Greenhouse Gas (GHG) [1] suggested that the share of vessel emissions in global anthropogenic GHG emissions increased from 2.76% (2012) to 2.89% (2018). The 2023 IMO Strategy on Reduction of GHG Emissions from Ships aimed to reach net-zero GHG emissions from international shipping close to 2050 [2]. Waste heat recovery for power generation was an excellent approach to achieve net-zero GHG emissions from shipping. The ORC reported the simple structure and high recovery efficiency in marine applications [3,4].

Recently, a large amount of attention focused on the ORC analysis on ships with exhaust gas (EG) waste heat sources. Battista et al. [5] studied the ORC at 50% of the M/E load. They recovered 3.5 kW of mechanical energy, which was equivalent to 5% of the M/E braking power. Baldi et al. [6] compared the optimization procedure of the ORC waste heat recovery based on the collection from a two-year operational profile of a chemical tanker. The results showed that the optimized installation of the ORC increased the vessel's fuel saving from 7.4% to 11.4%. Choi et al. [7] investigated an ORC system applied to exhaust gas discharged from the M/E of a 6800 TEU container ship. Yang et al. [8] reported the thermodynamic and economic performance of an ORC. Nawi et al. [9] examined the potential of an M/E exhaust waste heat recovery ORC system with bioethanol microalgae as the working fluid. Zhang et al. [10] carried out an experimental study on the waste heat recovery ORC under eight M/E operating conditions. He explored that various operational parameters significantly influenced the system performance. A container ship was selected for a case study about working fluid selection in ORC [11]. Geneidy et al. [12] studied the environmental impact of an operation-based ORC system for M/E waste heat recovery from an oil tanker. The results showed that the ORC system led to a 5.16% reduction in the total fuel consumption of the vessel. Lummen et al. [13] analyzed an ORC system for a passenger ferry, which operated on a short route.

Up to now, previous studies had highlighted factors such as the combination of heat sources, working fluid selection and thermo-economic performance. Several articles were performed by considering the different M/E load conditions. However, few studies applied the potential of waste heat recovery from the M/E under a voyage cycle, considering both the M/E load conditions and operating times. The investigation of waste heat recovery from ships based on the voyage cycle had more practical significance. Container ships had a variable operational profile during the voyage cycle, which directly affected the ORC potential. The study novelty stems from a voyage cycle-based waste heat utilization from the M/E was introduced to provide a reliable evaluation for proposing and designing ORC. The energetic, exergetic and environmental performance of an ORC system was estimated among different working fluid candidates. The voyage cycle of container ship M/V ZHONGGU DONGHAI was included to compare the M/E load conditions' and operating times' influence on the technical and environmental evaluation and working fluid selection of ORC.

2. System Description

2.1. The M/E and Waste Heat Source of EG Information

The MV ZHONGGU DONGHAI, a 1900 Twenty Feet Equivalent Unit (TEU) containership, was involved in this paper. The M/E for propulsion was QMD-WinGD 6RT-flex58T-E from Qingdao Haixi Heavy-duty machinery Co., Ltd. (Qingdao, China). The technical data of the marine M/E were represented in Table 1.

Table 1. Technical data of the marine M/E.

M/E Information at 100% Load	
M/E type	6RT-flex58T-E
Turbocharger type	A-165-L(ABB)
MCR Power (kW)	14,100
MCR Speed (rpm)	105
CSR Power (kW)	11,985
CSR Speed (rpm)	99.5
Piston Stroke (mm)	2416
Piston speed (m/s)	8.5
BSFC (g/kW h)	174
Scavenge air, mass flow (kg/s)	28.1
EG, mass flow (kg/s)	28.7
EG before the turbocharger, temperature (K)	752.15
EG after the turbocharger, temperature (K)	559.15
EG, density (kg/m^3)	0.641

The EG after the turbocharger was selected as waste heat for its reliability and validity. The 6RT-flex58T-E M/E output in terms of EG mass flow, temperature and BSFC with the M/E load factor were taken from engine manufacturer WIN GD [14], which was shown in Figures 1 and 2 and Table 2. The mass fraction compositions of the EG were O_2 (14.83%), N_2 (74.61%), CO_2 (4.36%) and H_2O (6.2%). The NO_X, SO_X and CO were all ignored because the fraction was too small. According to a calculation using REFPROP, the specific heat capacity of EG was approximately 1.089 kJ/(kg·K).

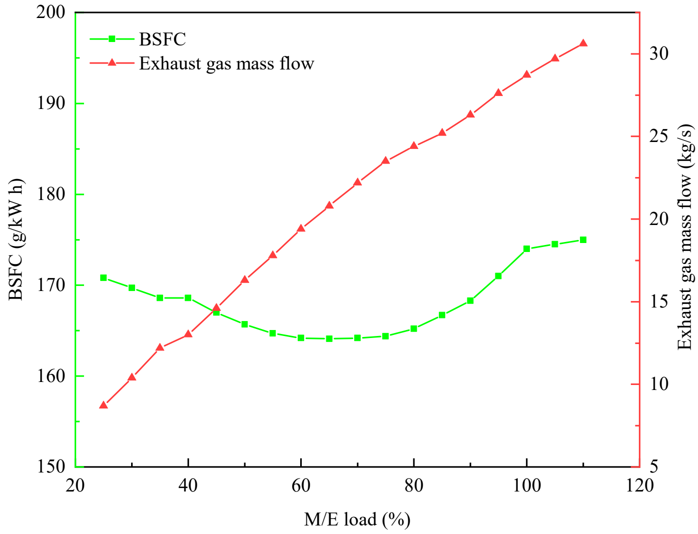

Figure 1. EG flow and BSFC versus M/E loads.

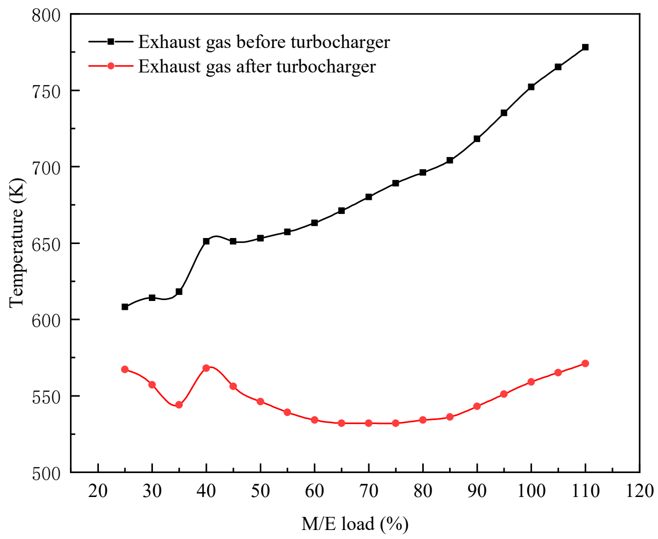

Figure 2. EG temperature versus M/E loads.

Table 2. Data of M/E and EG.

M/E Load (%)	M/E Power (kW)	Shaft Speed (rpm)	tEbT (K)	tEaT (K)	mExh (kg/s)
110	15,510	108.4	778.15	571.15	30.6
105	14,805	106.7	765.15	565.15	29.7
100	14,100	105	752.15	559.15	28.7
95	13,395	103.2	735.15	551.15	27.6
90	12,690	101.4	718.15	543.15	26.3
85	11,985	99.5	704.15	536.15	25.2
80	11,280	97.5	696.15	534.15	24.4
75	10,575	95.4	689.15	532.15	23.5
70	9870	93.2	680.15	532.15	22.2
65	9165	91	671.15	532.15	20.8
60	8460	88.6	663.15	534.15	19.4
55	7755	86	657.15	539.15	17.8

Table 2. *Cont.*

M/E Load (%)	M/E Power (kW)	Shaft Speed (rpm)	tEbT (K)	tEaT (K)	mExh (kg/s)
50	7050	83.3	653.15	546.15	16.3
45	6345	80.5	651.15	556.15	14.6
40	5640	77.4	651.15	568.15	13
35	4935	74	618.15	544.15	12.2
30	4230	70.3	614.15	557.15	10.4
25	3525	66.1	608.15	567.15	8.7

2.2. Working Fluids Selection

Available working fluids for ORC had wide varieties and different characteristics. The T–s diagrams of the different types of working fluids were shown in Figure 3, which was based on the commercial thermodynamic library REFPROP [15]. The saturation vapor curve was an important point that affected the suitability of the liquid, the arrangement of the equipment and the efficiency. Based on the subcritical ORC model, the most important criteria for the selection of the working fluid were critical temperature, high efficiency and low heat and humidity losses, which were ultimately determined by the EG situation and the thermodynamic properties of the working fluid.

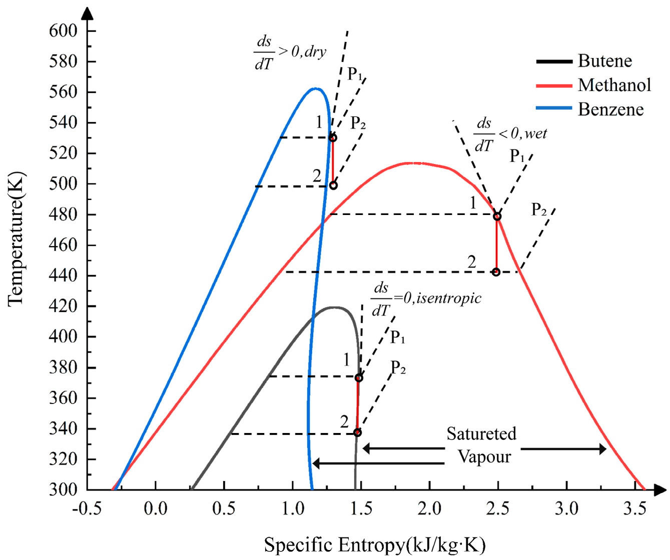

Figure 3. T–s diagram of the dry, wet and isentropic working fluids.

Yagli et al. [16] noted that the working fluids used in the ORC evaporated at a lower temperature than water, such as refrigerants, pentane, Toluene and Benzene. Kocaman et al. [17] discussed the performance of wet, isentropic and dry working fluids in the ORC. It was seen that dry-type working fluids were more feasible. Toluene was used as a working fluid in some high temperature ORC plants [18–20]. Siddiqi et al. [21] compared the performance of alkanes with water, Benzene and Toluene in the ORC with three heat source temperatures (773.15 K, 623.15 K and 523.15 K). The results show that hydrocarbons, such as n-hexane, were promising at the temperature range 523.15 K.

In this study, the EG temperature was in the range of 534.15–559.15 K, which was higher than the low temperature range in ORC systems. Due to this reason, the working fluids selected were Toluene, Benzene and Cyclohexane. The T–s diagrams of the three working fluids were shown in Figure 4 [15]. The slope of the saturation curve was positive, and the fluids were dry type, which had higher efficiency than wet ones [22]. The properties of the working fluids were listed in Table 3 [23–25].

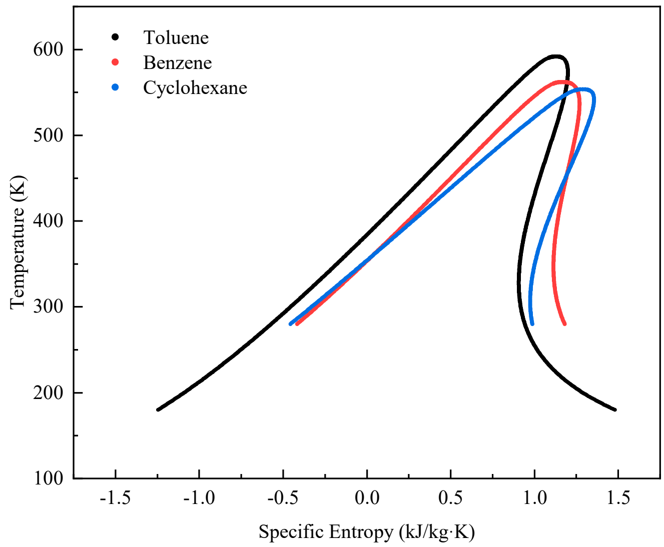

Figure 4. T–s diagram of the working fluids.

Table 3. Properties of the working fluids.

Name	Chemical Formula	GWP	ODP	Critical Pressure (kPa)	Critical Temperature (K)	Fluid Type
Toluene	C_7H_8	3	0	4126.3	591.75	Dry
Benzene	C_6H_6	~20	0	4907.3	562.02	Dry
Cyclohexane	C_6H_{12}	~20	0	4080.5	553.6	Dry

2.3. Voyage Cycle Overview

A 1900 TEU container liner involved in this work covered Thailand's Laem Chabang, Vietnam's Vung Tau-Saigon and China's Guangzhou-Ningbo-Shanghai, with about 20 days voyage time. In the present study, the data during the voyage cycle were collected. To increase the reliability of the navigation data, the Anchorage of Chang Jiang Kou was used as the starting point of the specific route. The navigation data were presented in Table 4. The shaft output power was inversely proportional to the third power of the ship at normal speed [26]. In order to carry out the calculations more accurately, a novel methodology was adopted. The shaft output power was converted from the M/E speed in the ship's engine log. The M/E power was equal to shaft output work.

Table 4. The navigation data.

Port	Voyage Time (h)	Shaft Speed (rpm)	M/E Load (%)	Fuel Consumption (g/kWh)	Power (kW)	EG Temperature (K)	EG Mass Flow (kg/s)
Changjiangkou	-	-	-	-	-	-	-
Shanghai	28.9	70.3	30%	169.7	4230	557.15	10.4
Ningbo	10.5	97.5	80%	165.2	11,280	534.15	24.4
Vung Tau	104.4	101.4	90%	168.3	12,690	543.15	26.3
Saigon	4.1	97.5	80%	165.2	11,280	534.15	24.4
Laem Chabang	44	99.5	85%	166.7	11,985	536.15	25.2
Guangzhou	110.3	97.5	80%	165.2	11,280	534.15	24.4
Shanghai	66.7	99.5	85%	166.7	11,985	536.15	25.2

3. Thermodynamic Analysis of ORC System

3.1. Thermodynamic Model

In this investigation, the ORC system contained five parts: an evaporator, an expander (turbine), a generator, a condenser and a pump. The layout of the ORC system was presented in Figure 5. The T–s diagram of the ORC was shown in Figure 6. The construction of Figure 6 was divided into three parts:

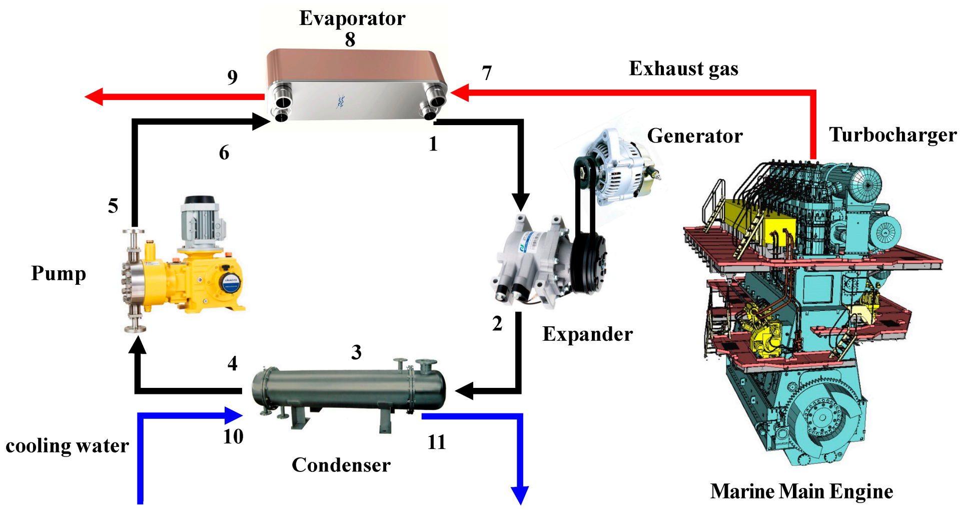

Figure 5. Layout of the ORC.

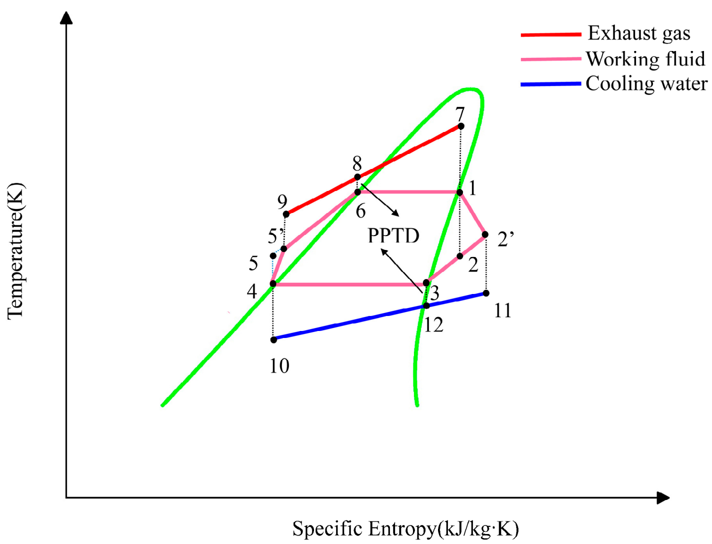

Figure 6. T–s diagram of the ORC.

1, Points 7–9 illustrated the EG heat transfer process at constant pressure.

2, Points 5–6–1–2–4–5 illustrated the working fluid thermodynamic process, which consisted of preheating (5–6), boiling (6–1), expansion (1–2), condensation (2–4) and pumping (4–5). Points 5 to 6 illustrated that the liquid organic working fluid could be preheated with EG. From Points 6 to 1, the working fluid absorbed heat from the EG, which was converted from a saturated liquid state to a saturated vapor or superheated vapor state. Points 1 to 2 indicated that the expanding of working fluid and the expander shaft produced power. Points 2 to 4 represented the process where the working fluid was cooled. Points 4–5 illustrated the compression process of the working fluid. Points 2′ and 5′ indicated the status points of the actual thermal process. Point 6 identified the starting point for boiling the working fluid. Points 8–6 indicated the pinch point temperature difference.

3, Points 10–11 illustrated the cooling water thermodynamic process at constant pressure.

At the vaporization start (Point 6) of the organic fluid, the difference between the vaporization temperature of the organic fluid and the exhaust temperature was considered to be the pinch point temperature difference (PPTD) [27]. The PPTD represented the limit of heat exchanger performance, i.e., evaporator and condenser. The temperature difference between Point 8 and Point 6 was assumed to be 6 K [28,29].

The first law analysis should be carried out to explore the energy balance. Moreover, the exergy analysis method was employed to evaluate the exergy utilization and exergy loss for low grade waste heat recovery.

The energy balance could be demonstrated in Equation (1).

$$Q_{\text{in}} = Q_{\text{out}} \tag{1}$$

The exergy flow change of the substance in the ORC system could be considered as:

$$\dot{E}_{\text{i}} = [(h_{\text{i-in}} - h_{\text{i-out}}) - T_0(s_{\text{i-in}} - s_{\text{i-out}})] \bullet \dot{m}_{\text{i}} \tag{2}$$

The energy and exergy equation of each component of the ORC was shown in Appendix A Table A1. The total energy rate flowing into the system was as follows:

$$\dot{E}_{\text{tot}} = \dot{E}_{\text{gas-wf}} + W_{\text{pump}} \tag{3}$$

The net power of the ORC could be calculated as follows:

$$W_{\text{net}} = W_{\text{exp}} - W_{\text{pump}} \tag{4}$$

The thermal efficiency of the ORC could be calculated as follows:

$$\eta_{1\text{st}} = \frac{W_{\text{net}}}{Q_{\text{gas}}} \tag{5}$$

The second-law efficiency of the power cycle, also referred to as exergy efficiency $\eta_{2\text{nd}}$, could be defined as follows:

$$\eta_{2\text{nd}} = \frac{W_{\text{exp}}}{\dot{E}_{\text{tot}}} \tag{6}$$

The total exergy that leaves the ORC system was defined as Equation (7).

$$\dot{I}_{\text{tot}} = \dot{I}_{\text{gas-wf}} + \dot{I}_{\text{exp}} + \dot{I}_{\text{cond}} + \dot{I}_{\text{cw}} + \dot{I}_{\text{pump}} \tag{7}$$

The expansion ratio of the expander was calculated as follows:

$$R_{\text{exp}} = \frac{P_{\text{evp}}}{P_{\text{con}}} \tag{8}$$

In order to evaluate the fuel saving from using ORC, R_{rp} was defined as the ratio between the recovered power from the ORC and the power of the M/E, which was calculated by Equation (9).

$$R_{\text{rp}} = \frac{W_{\text{net}}}{W_{\text{ship}}} \tag{9}$$

where W_{ship} meant the power of the M/E.

The fuel saving from using ORC was calculated by Equation (10).

$$M_{\text{fs}} = W_{\text{net}} \times \text{BSFC} \times H, \tag{10}$$

where H meant the running hours of the ORC system.

According to IMO MEPC (Marine Environment Protection Committee), the conversion factor between fuel consumption and CO_2 emission C_F was defined as 3.114 g CO_2/g Fuel [30], which was suited for diesel ships and included HFO (heavy fuel oil) used in practice.

$$M_{CO_2} = M_{fs} \times C_F \tag{11}$$

In particular, for those engines that did not have a test report included in the NOx Technical File and that did not have the specific fuel consumption from the manufacturer, carbon factor estimation accuracy was credible considering the real exploitation conditions.

3.2. Assumptions and Validation

Before the investigation, the systems were assumed to operate under steady-state condition. The heat and resistance losses in components and piping were neglected. The isentropic efficiency of the expander and pump was 0.8. The condensation pressure was 102 kPa. The pinch points in the heat exchanger were no less than 6 K, and the EG outlet temperature was above 375 K. The dead state temperature was assumed to be 290 K (T_0).

A comparison of the simulation results with the experimental data [31] was shown in Table 5, which compared the performance of the system with Cyclohexane as the working fluid. The results indicated that the maximum relative error was 3.7%, which was within the permissible range. As a result, the rationality of the system model can be effectively verified.

Table 5. The validation data with Cyclohexane as working fluid.

Parameters	Experimental Data	Simulation Data	Error
The isentropic efficiency of the expander	0.8	0.8	-
The isentropic efficiency of the pump	0.8	0.8	-
PPTD (K)	6	6	-
The EG mass flow rate (kg/h)	7139	7139	-
The EG inlet temperature (K)	573.15	573.15	-
The specific heat capacity of the EG (kJ/(kg·K))	1.1	1.089	1%
The Evaporation temperature (K)	480.3	480.3	-
The condensation temperature (K)	355	355	-
Net power (kW)	64	65.47	2.2%
Thermal efficiency (%)	14.8	15.25	2.9%
Mass flow (kg/s)	0.8	0.77	3.7%

4. Results and Discussion

4.1. Net Power and the Exhaust Outlet Temperature

The waste heat EG had variable parameters under different M/E loads, and three different working fluids were selected in this study; both were directly affected the ORC potential. The first set of analyses examined the impact of an M/E load on the thermodynamic performance of ORC. In particular, for going deeper in the physical interpretation of different working fluid results by considering non-dimensional numbers, a correspondence state parameter was defined as the ratio of evaporative pressure to critical pressure (RECP).

Figure 7a compared changes in the net power and RECP at 90% load. It could be seen from the data in Figure 7a that a trend in the net power was increasing and decreasing with RECP. Meanwhile, at an RECP of 16% (Toluene), 21% (Benzene) or 25.3% (Cyclohexane), the highest net power was 373.4 kW (Toluene), 584.1 kW (Benzene) or 605.8 kW (Cyclohexane). Several factors were known to play a role in determining the net power. When the evaporation pressure of the working fluid increased, the enthalpy of the working fluid also increased while the mass flow rate of the working fluid decreased, which changed at an inconsistent rate. Therefore, the highest net power could be obtained with RECP. The single most striking observation to emerge from the data comparison was that Cyclohexane had the highest net power of 605.8 kW, followed by Benzene and Toluene at the same evaporation pressure. A closer inspection of Figure 7b showed that the highest net power was 323.3 kW (Toluene), 513.2 kW (Benzene) and 530.5 kW (Cyclohexane).

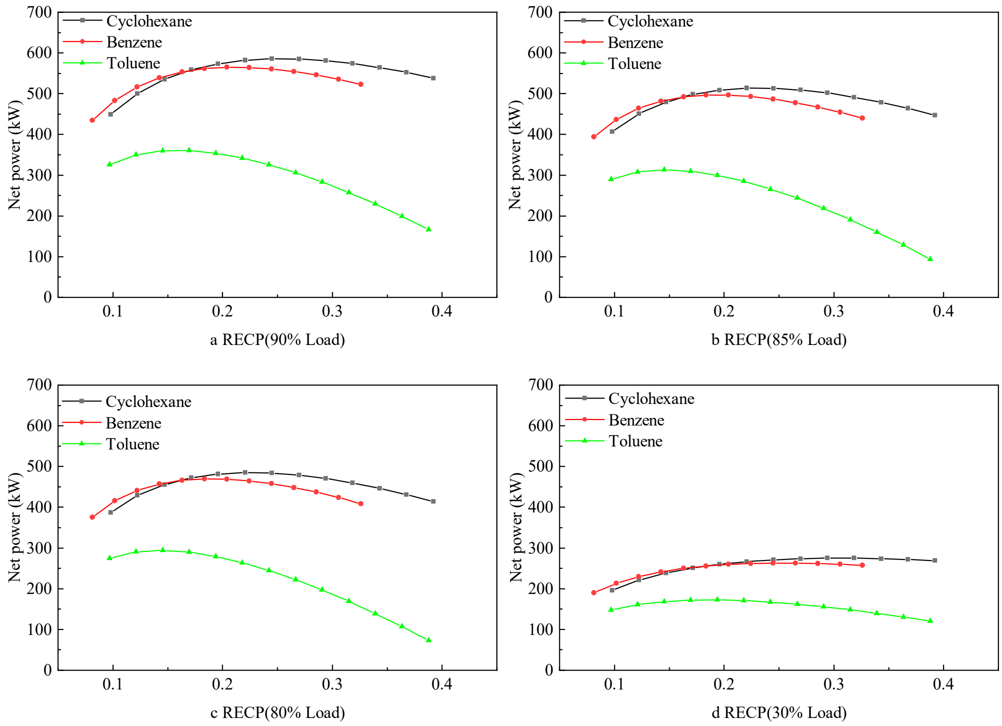

Figure 7. The changes in the net power and RECP versus different M/E loads (**a**) were the changes in the net power and RECP at 90% load, (**b**) were the changes in the net power and RECP at 85% load, (**c**) were the changes in the net power and RECP at 80% load and (**d**) were the changes in the net power and RECP at 30% load.

The preliminary analysis of Figure 7a,b was validated by Figure 7c,d. A possible explanation for these results may be that the EG mass flow rate decreased as the M/E's load decreased. Although the temperature of the EG increased at a 30% load, the mass flow rate dropped significantly, which led to a decrease in the residual heat of the EG. This finding was expected and suggested that the same characteristics of a positive correlation were found between the highest net power and M/E load. Together these results provided important insights into when the more significant the M/E load was, as it was then more suitable for waste heat recovery.

To avoid acid dew points, the EG outlet temperature must be above 375 K. On the other hand, the EG outlet temperature also represented the degree of waste heat utilization. A positive correlation was found between the EG outlet temperature and the RECP, which was shown in Figure 8. It could be seen from the data in Figure 8a that when the RECP was 16% (Toluene), 21% (Benzene) or 25% (Cyclohexane), the EG outlet temperature was 429.3 K (Toluene), 402.7 K (Benzene) or 389.7 K (Cyclohexane).

These factors may explain the relatively good correlation between the EG outlet temperature and the RECP. The evaporator could be divided into preheating and boiling areas in the ORC cycle. As the evaporation pressure rose in the boiling section, the evaporation temperature also rose correspondingly. The pinch point moved toward the EG inlet. Since the flow rate of the EG remained constant, the working fluid flow rate decreased according to Equation (2). In the preheating section, the temperature and pressure of the condensed mass remained constant because the condensing pressure was assumed to be 102 kPa. After compression by the pump, the temperature and pressure of the working fluid did not change. The reduction of the mass flow rate led to a reduction of the demanded exhaust residual heat. They combined the above factors and the exhaust outlet temperature increased. Data from Figure 8a could be compared with the data in Figure 8b–d, which showed two results: For a single working fluid, the exhaust outlet temperature was highest at a 30% load and lowest at an 80% load. At the same M/E load, the exhaust outlet temperature of Toluene was the highest, Benzene was the second and Cyclohexane was the lowest.

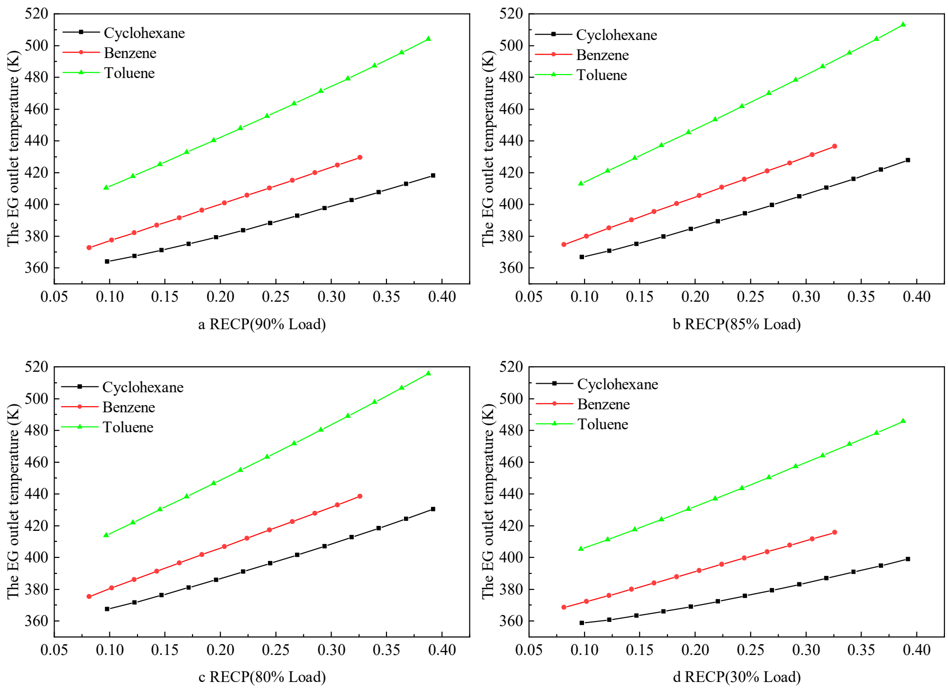

Figure 8. The correlation between EG outlet temperature and the RECP (**a**) was the correlation between EG outlet temperature and RECP at 90% load, (**b**) was the correlation between EG outlet temperature and RECP at 85% load, (**c**) was the correlation between EG outlet temperature and RECP at 80% load and (**d**) was the correlation between EG outlet temperature and RECP at 30% load.

The ORC system parameters differed significantly when the different working fluid was selected. For example, Cyclohexane had an advantage in net power, Benzene had an advantage in thermal efficiency and Toluene had an advantage in the EG outlet temperature. The sensitivity of ORC system performance parameters varied with the M/E load. The most striking result from the data was that the net power was more sensitive than the thermal efficiency and exhaust outlet temperature.

Appendix A Table A2 showed the results of the ORC system with three working fluids. At a 90% load, the highest net power in the ORC system was 605.75 kW (Cyclohexane), the highest thermal efficiency was 14.56% (Benzene) and the exhaust outlet temperature was 429.3 K (Toluene). At an 85% load, the highest net power in the ORC system was 530.48 kW (Cyclohexane), the highest thermal efficiency was 14.14% (Benzene) and the exhaust outlet temperature was 429.44 K (Toluene). At an 80% load, the highest net power in the ORC system was 500.41 kW (Cyclohexane), the highest thermal efficiency was 14.01% (Benzene) and the exhaust outlet temperature was 429.47 K (Toluene). At a 30% load, the highest net power in the ORC system was 285.03 kW (Cyclohexane), the highest thermal efficiency was 15.43% (Benzene) and the exhaust outlet temperature was 428.38 K (Toluene).

4.2. Exergy Flow Losses and Exergy Efficiency

The exergy analysis was employed to recognize parts of the ORC system where irreversibility occurs and was essential for a comprehensive evaluation of the ORC system. Among the three working fluids, Cyclohexane was selected for the observation. Four items of exergy flow losses of the ORC system at the 80% and 30% M/E load with Cyclohexane were shown in Figure 9. They were, sequentially, (1) Evaporator $\dot{I}_{gas-wf}$, (2) Expander $\dot{I}_{exp}$, (3) Condenser $\dot{I}_{cond}$, (4) Pump $\dot{I}_{\mathrm{pump}}$.

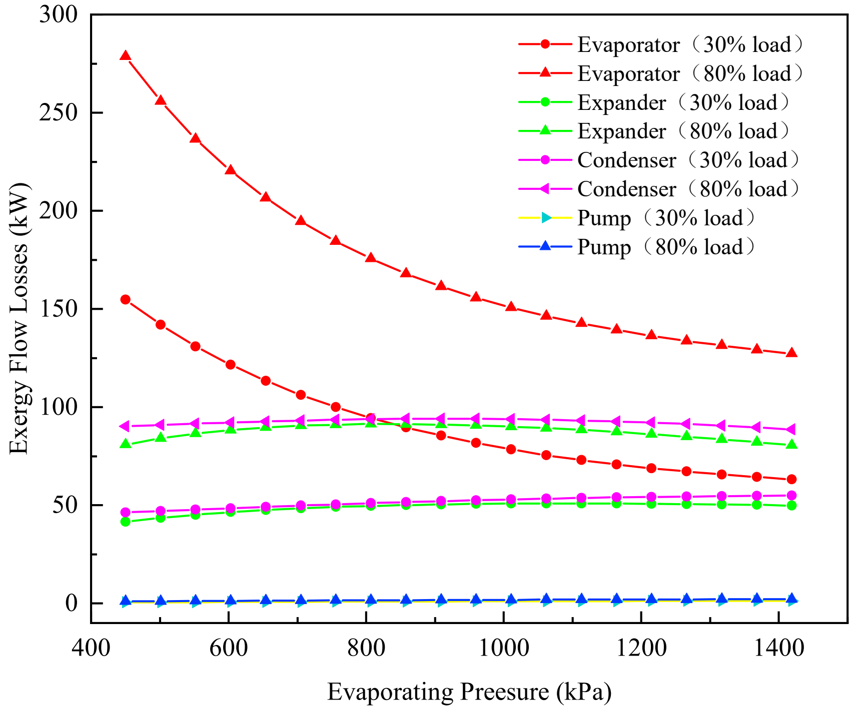

Figure 9. Four items of exergy flow losses.

The exergy flow loss in the evaporator $\dot{I}_{gas-wf}$ showed a decreasing trend as the evaporation pressure increased while the others remained a slight constant. Due to the growth of the evaporation temperature, the temperature difference between the EG and working fluid gradually decreased, reducing the irreversibility of the evaporator. The mass flow rate decreased simultaneously with the increase in evaporation pressure. While the entropy difference between the expander and the pump increased, the exergy flow loss $\dot{I}_{exp}$ and $\dot{I}_{\mathrm{pump}}$ did not change much. Meanwhile, the condensing pressure of the system was set at 102 kPa, and the cooling water inlet temperature was set at 333.15 K. The temperature difference and flow rate difference of the condenser changed simultaneously, and the $\dot{I}_{cond}$ remained stable. At an evaporation pressure of 922 kPa under an 80% load, the above four items of exergy flow losses of the ORC system were 159.8 kW, 94 kW, 91 kW and 1.7 kW, respectively. Among the ORC items, $\dot{I}_{gas-wf}$ was the highest, followed by $\dot{I}_{\mathrm{cond}}$, $\dot{I}_{exp}$ and $\dot{I}_{\mathrm{pump}}$. Consequently, it was indispensable to optimize the evaporator and condenser to reduce the exergy flow losses.

Compared to the energy analysis, exergy efficiency and flow losses could provide a deeper understanding in the effectiveness of an energy resource utilization system. The influence on system exergy efficiency and flow losses under different M/E loads and evaporating pressures was presented in Figure 10. The arrow pointing to the left represented the exergy efficiency, the arrow pointing to the right represented the total exergy flow loss.

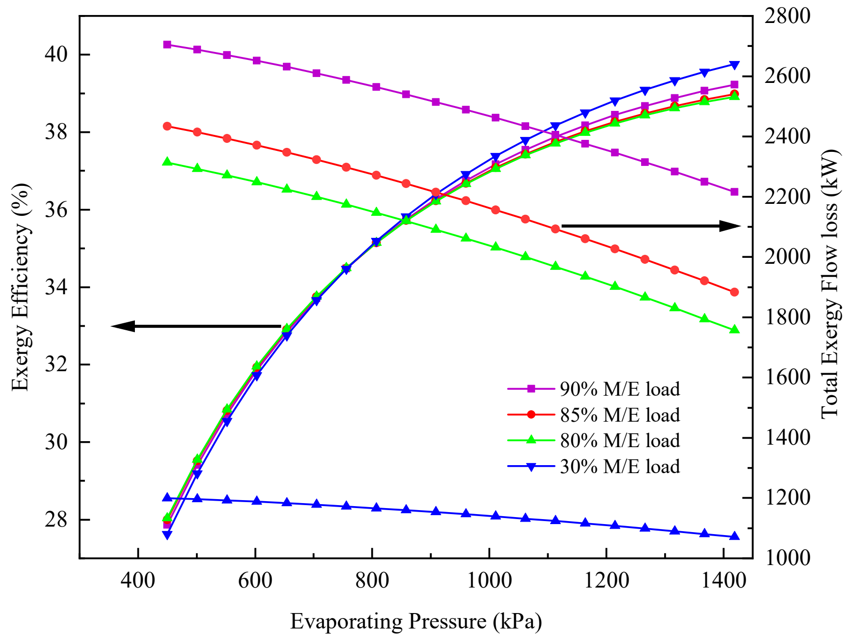

Figure 10. Exergy efficiency and total Exergy flow loss variation with Cyclohexane.

First, the drop in the M/E load (from 90% to 30%) led to the reduction in the waste heat of the EG, and as a consequence, the total exergy flow loss of the ORC system fell. Second, the exergy efficiency presented a non-significant trend, which was due to the fact that the EG was adopted as waste heat resources in this investigation after the turbocharger, and its temperature was respectively 543.15 K (90% M/E load), 536.15 K (85% M/E load), 534.15 K (80% M/E load) and 557.15 K (30% M/E load). According to Equation (6), the regularity of exergy efficiency was based on expansion power and the total exergy flow loss under certain conditions by comparing Figure 8. Third, the EG temperature played a vital role in the exergy efficiency, which was highest at a 30% M/E load, followed by a 90%, 85% and 80% M/E load.

4.3. Working Fluids Performance during the Voyage Cycle

The EG temperature and flow rate changed during the voyage cycle. It was essential to refine the parameters of the ORC system to obtain the highest net output power. According to Ref. [32], the evaporation pressure and flow rate of the ORC system could be controlled by adjusting the frequency and displacement of the pump. However, the time of the route changed in different routes. It was significant to analyze the evaporation pressure and mass flow rate of the ORC system during the voyage cycle, which would help to discover the regulation of ORC in the actual voyage of the vessel.

The evaporation pressures of different routes were presented in Figure 11. The evaporation pressures in the first route were 1248 kPa (Cyclohexane), 1235 kPa (Benzene) and 769 kPa (Toluene), which was the highest of the seven routes. A possible explanation for this might be that the EG temperature was highest at 30%M/E load. Based on the PPTD, the working fluid could be optimized to a higher evaporation temperature and pressure. Nevertheless, the optimal evaporation pressures in the second route were 922 kPa (Cyclohexane), 932 kPa (Benzene) and 592 kPa (Toluene), which were the lowest of the seven routes. Another possible explanation for this was that the M/E load was 80% and the temperature of the EG was 534.15 K. With the limitation of the temperature difference of the pinch point, very high evaporation temperatures and pressures could not be obtained. The same pattern was shown in the other routes. A further analysis showed that the evaporation pressures need to be adjusted to keep the ORC system performing optimally at different M/E loads.

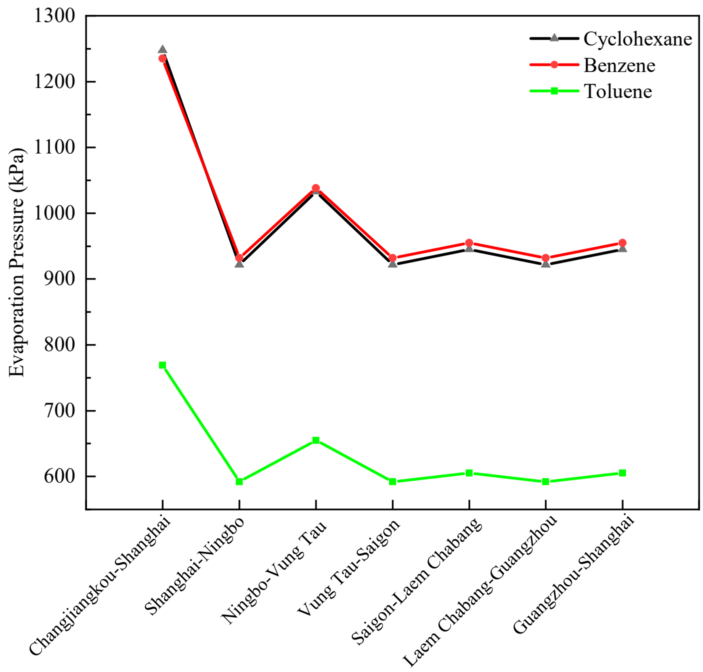

Figure 11. The evaporation pressures of different routes.

The mass flow rates of different routes were shown in Figure 12. The mass flow rates in the first route were 3.64 kg/s (Cyclohexane), 3.35 kg/s (Benzene) and 2.99 kg/s (Toluene), which was the lowest of the seven routes. It may have something to do with the EG temperature and EG flow rate due to the fact that the M/E load was 30%. On the one hand, the higher EG temperature led to a higher evaporation pressure. On the other hand, the lower EG flow rate led to a lower total EG heat. When the M/E load was 90%, the EG temperature and flow rate both increased substantially so that the flow rate of the working fluid also increased significantly. Overall, these results indicated that the mass flow rates of the working fluid should be consistent with the M/E load, which would provide a reference for the application of ORC technology on a real vessel.

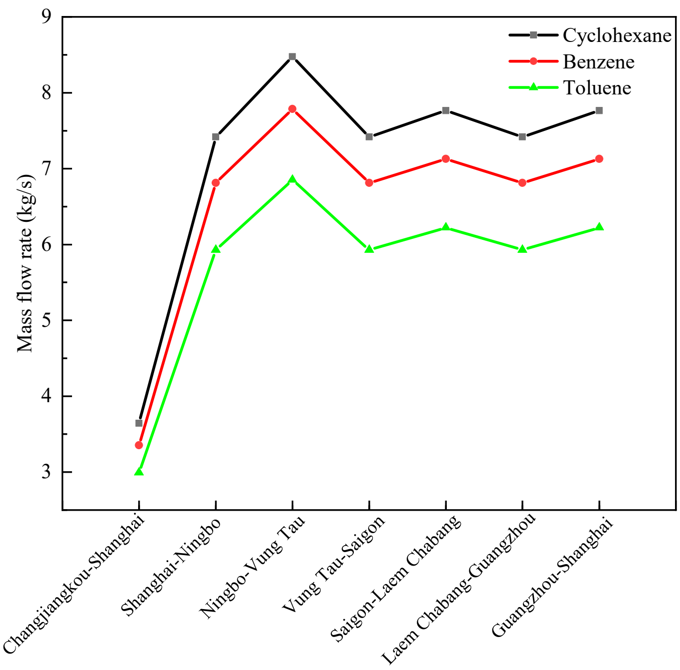

Figure 12. The mass flow rates of different routes.

4.4. Environmental Performance

The CO_2 emissions in different routes were compared in Figure 13. The CO_2 emissions in the first route were 4.33 tons (Cyclohexane), 4.15 tons (Benzene) and 2.72 tons (Toluene), respectively. It seems possible that these results were due to the max net power and were 285.03 kW (Cyclohexane), 272.73 kW (Benzene) and 178.79 kW (Toluene), and the route time was 28.9 h. The CO_2 emissions in the second route were 2.69 tons (Cyclohexane), 2.61 tons (Benzene) and 1.63 tons (Toluene). These results were likely to be related to the max net power was 500.4 kW (Cyclohexane), 484.57 kW (Benzene), 429.48 kW (Toluene) and the route time was 10.5 h. Data from the first route could be compared with the data in the second route, which showed a positive correlation between CO_2 emission and route time. The CO_2 emissions in the third route were 32.99 tons (Cyclohexane), 31.82 tons (Benzene) and 20.34 tons (Toluene), which were the max among the seven routes. The max net power was 605.75 kW (Cyclohexane), 584.14 kW (Benzene) and 373.45 kW (Toluene), and the route time was 104.4 h. However, the CO_2 emissions in the fourth route only were 1.05 tons (Cyclohexane), 1.02 tons (Benzene) and 0.64 tons (Toluene). It could be assumed that route time played an important role in addressing the issue of CO_2 emissions. According to these data, it was more profitable to use the ORC system on long routes during voyage cycle. It was interesting to note that the total CO_2 emissions were 99.68 tons (Cyclohexane), 96.32 tons (Benzene) and 60.99 tons (Toluene) in all seven routes in this study. Detailed parameters during the voyage cycle were shown in Appendix A Table A3.

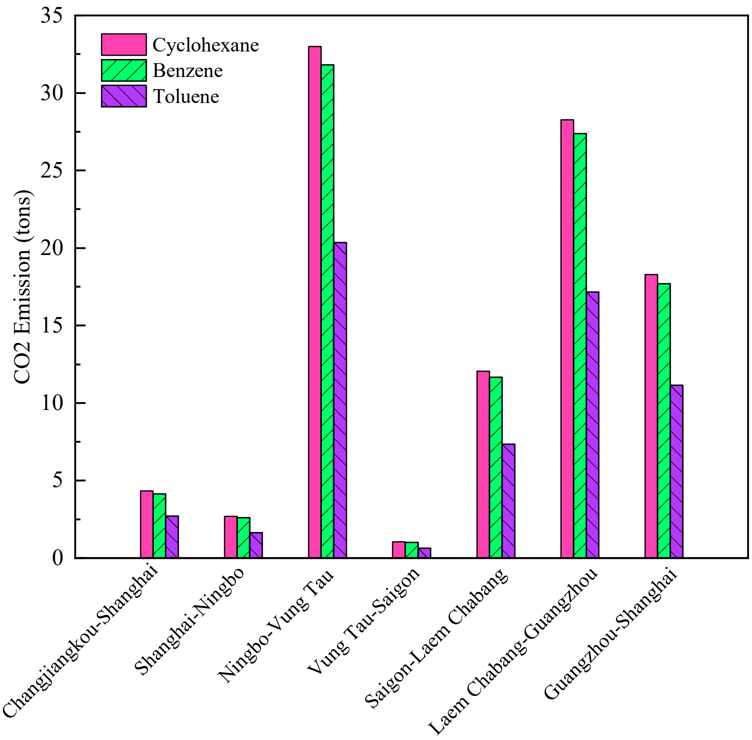

Figure 13. The CO_2 emission of different routes.

5. Conclusions

In this paper, a voyage cycle-based waste heat utilization from the M/E was introduced to provide reliable evaluation for proposing and designing a thermodynamic ORC model. The effect of various M/E loads on the energy and exergy performance of ORC was analyzed among three dry-type substances. The environmental analysis was presented based on the measurement data from one voyage cycle navigation of an objective container ship. The conclusions could be gained as follows:

1. The ORC system parameters had significant differences versus the different working fluids. The highest net power in the ORC system was 605.75 kW at a 90% M/E load

(Cyclohexane), the highest thermal efficiency was 15.43% at a 30% M/E load (Benzene) and the exhaust outlet temperature was 429.5 K at an 80% M/E load. Cyclohexane had an advantage in net power, Benzene had an advantage in thermal efficiency and Toluene had an advantage in the EG outlet temperature. The sensitivity of ORC system performance parameters varied when the M/E load changed.

2. The exergy flow losses of the ORC system were 159.8 kW (evaporator), 94 kW (condenser), 91 kW (expander) and 1.7 kW (pump) at an evaporation pressure of 922 kPa under an 80% M/E load with Cyclohexane. The evaporator was the highest, followed by the condenser, expander and pump. It was indispensable to optimize the evaporator and condenser to reduce the irreversibility of ORC systems.

3. The evaporation pressures of ORC during the voyage cycle were 922–1248 kPa (Cyclohexane), 932–1235 kPa (Benzene) and 592–769 kPa (Toluene). The evaporation pressure needed to be adjusted to keep the ORC system performing optimally at different M/E loads. The working fluid flow rates in the ORC were from 3.64–8.47 kg/s(Cyclohexane), 3.35–7.79 kg/s (Benzene) and 2.99–6.85 kg/s (Toluene). The mass flow rates of the working fluid should be consistent with the M/E load, which would provide a reference for the application of ORC technology on the real vessel.

4. The CO_2 emissions during the voyage cycle were 99.68 tons (Cyclohexane), 96.32 tons (Benzene) and 60.99 tons (Toluene). The route time played an important role in addressing the issue of CO_2 emission.

The optimization for the system's evaporator and condenser must be conducted to reduce the irreversibility of ORC systems in the future. Working fluid selection and designing parameters shall be carried out to further improve the energy efficiency for container ships. Moreover, the experiment with ORC technology on board shall be taken to achieve a more reliable assessment of the application of ORC systems based on the voyage cycle.

Author Contributions: Investigation, L.L.; Formal analysis, B.F.; Methodology, A.K. and Y.Z.; Project administration, W.C.; Resources, B.F.; Validation, Y.Z.; Writing—original draft, L.L.; Writing—review & editing, A.K. All authors have read and agreed to the published version of the manuscript.

Funding: This research was funded by the Science and Technology Plan Project of Jiangsu maritime institute (grant number 2022kjcx-03); Thousand Sails New Talent Program of Jiangsu maritime institute (grant number 2021qfxr); National Natural Sciences Foundation of China (grant numbers U2167214). The authors would like to render thankfulness to the Groups W G D, Ltd. for the materials supply.

Institutional Review Board Statement: Not applicable.

Informed Consent Statement: Not applicable.

Data Availability Statement: The data sets supporting the conclusions of this article are included within the article and the sequencing data correspond with Figures. It will be made available up-on reasonable academic request within the limitations of informed consent by the corresponding author upon acceptance.

Conflicts of Interest: No conflict of interest exists in the submission of this manuscript, and the manuscript is approved by all authors for publication.

Nomenclature

Acronyms		**Subscripts**	
BSFC	Brake specific fuel consumption	boil	Boiling process
CSR	Continuous service rating	con	Condenser
C	Carbon factor	exp	Expander
EG	Exhaust gas	eva	Evaporation process
GWP	Global warming potential	gas	Exhaust gas
MCR	Maximum Continuous Power	PPTD	Pinch point temperature difference
M/E	Main engine	pre	Preheating process

ORC	Organic Rankine cycle	the	Thermal
ODP	Ozone depletion potential	tot	Total
RECP	Ratio between evaporation pressure and critical pressure	wf	Working fluid
R	Ratio	fs	Fuel saving
tEbT	Temperature of exhaust gas before turbocharger	rp	Recovered power
tEaT	Temperature of exhaust gas after turbocharger		
H	Hour		
Nomenclature		**Greek symbols**	
Cp	Specific heat capacity (kJ/(kg·K))	η	Efficiency
$\dot{E}$	Exergy (kW)		
I	Exergy loss (kW)		
h	Specific enthalpy (kJ/kg)		
$\dot{m}$	Mass flow rate (kg/s)		
P	Pressure (kPa)		
Q	Heat power (kW)		
S	Entropy (kJ/K)		
T	Temperature (K)		
W	Power (kW)		
M	Mass (t)		

Appendix A

Table A1. The Energy and Exergy Equation of Each Component of the ORC.

Components	Energy	Exergy	Isentropic Efficiency
EG	$Q_{\text{gas}} = \dot{m}_{\text{gas}} \cdot c_{\text{P,gas}} \cdot (T_{\text{gas,7}} - T_{\text{gas,9}})$	$\dot{E}_{\text{gas}} = [(h_{\text{gas,7}} - h_{\text{gas,9}}) - T_0(s_{\text{gas,7}} - s_{\text{gas,9}})] \bullet \dot{m}_{\text{gas}}$	
Evaporator preheating	$Q_{\text{pre}} = \dot{m}_{\text{wf}} \cdot (h_6 - h_{5\prime})$	$\dot{I}_{\text{gas-wf}} = \left(\dot{E}_{\text{gas,7}} - \dot{E}_{\text{gas,9}}\right) - \left(\dot{E}_1 - \dot{E}_{5\prime}\right)$	
Evaporator boiling	$Q_{\text{boil}} = \dot{m}_{\text{wf}} \cdot (h_1 - h_6)$		
Expander	$W_{\text{exp}} = \dot{m}_{\text{wf}} \cdot (h_1 - h_{2\prime})$	$\dot{I}_{\text{exp}} = T_0(s_{2\prime} - s_1) \bullet \dot{m}_{\text{wf}}$	$\eta_{\text{exp}} = \frac{h_1 - h_{2\prime}}{h_1 - h_2}$
Condenser	$Q_{\text{con}} = \dot{m}_{\text{wf}} \cdot (h_{2\prime} - h_4)$	$\dot{I}_{\text{cond}} = (E_{2\prime} - E_4) - \left(\dot{E}_{11} - \dot{E}_{10}\right)$	
Cooling water	$Q_{\text{cw}} = \dot{m}_{\text{cw}} \cdot (h_{11} - h_{10})$	$\dot{I}_{\text{cw}} = \dot{E}_{\text{cw}} = [(h_{11} - h_{10}) - T_0(s_{11} - s_{10})] \bullet \dot{m}_{\text{cw}}$	
Pump	$W_{\text{pump}} = \dot{m}_{\text{wf}} \cdot (h_{5\prime} - h_4)$	$\dot{I}_{\text{pump}} = T_0(s_{5\prime} - s_4) \bullet \dot{m}_{\text{wf}}$	$\eta_{\text{pump}} = \frac{h_5 - h_4}{h_{5\prime} - h_4}$

Table A2. The Main Characteristics of the ORC Systems.

Load	90% Load			85% Load			80% Load			30% Load		
working fluid	Cyclohexane	Benzene	Toluene	Cyclohexane	Benzene	Toluene	Cyclohexane	Benzene	Toluene	Cyclohexane	Benzene	Toluene
evap (kPa)	1033	1038	655	945	955	605	922	932	592	1248	1235	769
conp (kPa)	102	102	102	102	102	102	102	102	102	102	102	102
exp ratio	10.13	10.18	6.42	9.26	9.36	5.93	9.04	9.14	5.80	12.24	12.11	7.54
R_{rp}	4.7%	4.6%	2.9%	4.4%	4.2%	2.7%	4.4%	4.2%	2.7%	8%	7.7%	5%
RECP	25%	21%	16%	23%	19%	14.8%	23%	19%	14%	31%	25%	19%
Net power (kW)	605.8	584.1	373.4	530.5	513.2	323.3	500	484.6	303.9	285	272.7	178.7
EG outlet tem (K)	389.7	402.7	429.3	391.6	403.3	429.4	392.1	403.4	429.5	384.9	401	428.4
Thermal efficiency	13.8%	14.6%	11.4%	13.4%	14%	11%	13.3%	14%	11%	14.6%	15.4%	12.3%
Mass flow rate (kg/s)	8.47	7.79	6.85	7.76	7.13	6.22	7.42	6.81	5.93	3.64	3.35	2.99

Table A3. Detailed Parameters during Voyage Cycle.

Parameters	Fluid	Changjiangkou–Shanghai	Shanghai–Ningbo	Ningbo–Vung Tau	Vung Tau–Saigon	Saigon–Laem chabang	Laem chabang–Guangzhou	Guangzhou–Shanghai
Expander ratio	Cyclohexane	12.24	9.04	10.13	9.04	9.26	9.04	9.26
	Benzene	12.11	9.14	10.18	9.14	9.36	9.14	9.36
	Toluene	7.54	5.8	6.42	5.8	5.93	5.8	5.93

Table A3. *Cont.*

Parameters	Fluid	Changjiangkou–Shanghai	Shanghai–Ningbo	Ningbo–Vung Tau	Vung Tau–Saigon	Saigon–Laem chabang	Laem chabang–Guangzhou	Guangzhou–Shanghai
Mass flow rate (kg/s)	Cyclohexane	3.64	7.42	8.47	7.42	7.76	7.42	7.76
	Benzene	3.35	6.81	7.79	6.81	7.13	6.81	7.13
	Toluene	2.99	5.93	6.85	5.93	6.22	5.93	6.22
Thermal efficiency (%)	Cyclohexane	14.6	13.3	13.8	13.3	13.4	13.3	13.4
	Benzene	15.4	14	14.6	14	14.1	14	14.1
	Toluene	12.3	11	11.5	11	11.1	11	11.1
Voyage Time (h)	Cyclohexane	28.9	10.5	104.4	4.1	44	110.3	66.7
	Benzene	28.9	10.5	104.4	4.1	44	110.3	66.7
	Toluene	28.9	10.5	104.4	4.1	44	110.3	66.7
Net power (kW)	Cyclohexane	285.03	500.41	605.75	500.41	530.48	500.41	530.48
	Benzene	272.73	484.57	584.14	484.57	513.24	484.57	513.24
	Toluene	178.79	303.89	373.45	303.89	323.32	303.89	323.32
Fuel saving (tons)	Cyclohexane	1.4	0.87	10.64	0.34	3.89	9.12	5.90
	Benzene	1.34	0.84	10.26	0.33	3.76	8.83	5.71
	Toluene	0.88	0.53	6.56	0.21	2.37	5.54	3.59
CO_2 (tons)	Cyclohexane	4.33	2.69	32.99	1.05	12.06	28.27	18.29
	Benzene	4.15	2.61	31.82	1.02	11.67	27.37	17.69
	Toluene	2.72	1.63	20.34	0.64	7.35	17.17	11.14

References

1. Zhu, L. A questionnaire based study on the status quo and future action over the regulation of marine greenhouse gas emissions in Hong Kong. *Mar. Policy* **2022**, *145*, 105278. [CrossRef]
2. IMO Marine Environment Protection Committee (MEPC 80). Available online: https://www.imo.org/en/MediaCentre/MeetingSummaries/Pages/MEPC-80.aspx (accessed on 3 July 2023).
3. Mahmoudi, A.; Fazli, M.; Morad, M.R. A recent review of waste heat recovery by Organic Rankine Cycle. *Appl. Therm. Eng.* **2018**, *143*, 660–675. [CrossRef]
4. Mondejar, M.E.; Andreasen, J.G.; Pierobon, L.; Larsen, U.; Thern, M.; Haglind, F. A review of the use of organic Rankine cycle power systems for maritime applications. *Renew. Sustain. Energy Rev.* **2018**, *91*, 126–151. [CrossRef]
5. Di Battista, D.; Di Bartolomeo, M.; Cipollone, R. Full energy recovery from exhaust gases in a turbocharged diesel engine. *Energy Convers. Manag.* **2022**, *271*, 116280. [CrossRef]
6. Baldi, F.; Larsen, U.; Gabrielii, C. Comparison of different procedures for the optimisation of a combined Diesel engine and organic Rankine cycle system based on ship operational profile. *Ocean. Eng.* **2015**, *110*, 85–93. [CrossRef]
7. Choi, B.C.; Kim, Y.M. Thermodynamic analysis of a dual loop heat recovery system with trilateral cycle applied to exhaust gases of internal combustion engine for propulsion of the 6800 TEU container ship. *Energy* **2013**, *58*, 404–416. [CrossRef]
8. Yang, M.-H.; Yeh, R.-H. Thermodynamic and economic performances optimization of an organic Rankine cycle system utilizing exhaust gas of a large marine diesel engine. *Appl. Energy* **2015**, *149*, 1–12. [CrossRef]
9. Mat Nawi, Z.; Kamarudin, S.K.; Sheikh Abdullah, S.R.; Lam, S.S. The potential of exhaust waste heat recovery (WHR) from marine diesel engines via organic rankine cycle. *Energy* **2019**, *166*, 17–31. [CrossRef]
10. Zhang, X.; Wang, X.; Cai, J.; He, Z.; Tian, H.; Shu, G.; Shi, L. Experimental study on operating parameters matching characteristic of the organic Rankine cycle for engine waste heat recovery. *Energy* **2022**, *244*, 122681. [CrossRef]
11. Gürgen, S.; Altın, İ. Novel decision-making strategy for working fluid selection in Organic Rankine Cycle: A case study for waste heat recovery of a marine diesel engine. *Energy* **2022**, *252*, 124023. [CrossRef]
12. El Geneidy, R.; Otto, K.; Ahtila, P.; Kujala, P.; Sillanpää, K.; Mäki-Jouppila, T. Increasing energy efficiency in passenger ships by novel energy conservation measures. *J. Mar. Eng. Technol.* **2017**, *17*, 85–98. [CrossRef]
13. Lümmen, N.; Nygård, E.; Koch, P.E.; Nerheim, L.M. Comparison of organic Rankine cycle concepts for recovering waste heat in a hybrid powertrain on a fast passenger ferry. *Energy Convers. Manag.* **2018**, *163*, 371–383. [CrossRef]
14. WIN GD. WinGD's General Technical Data (GTD). Available online: https://www.wingd.com/en/engines/general-technical-data-(gtd)/ (accessed on 15 September 2023).
15. Lemmon, E.W.; Huber, M.L.; McLinden, M.O. *NIST Standard Reference Database 23: Reference Fluid Thermodynamic and Transport Properties-REFPROP, Version 9.1*; National Institute of Standards and Technology: Gaithersburg, MD, USA. Available online: https://tsapps.nist.gov/publication/get_pdf.cfm?pub_id=912382 (accessed on 21 October 2023).
16. Yağlı, H.; Koç, Y.; Kalay, H. Optimisation and exergy analysis of an organic Rankine cycle (ORC) used as a bottoming cycle in a cogeneration system producing steam and power. *Sustain. Energy Technol. Assess.* **2021**, *44*, 100985. [CrossRef]
17. Kocaman, E.; Karakuş, C.; Yağlı, H.; Koç, Y.; Yumrutaş, R.; Koç, A. Pinch point determination and Multi-Objective optimization for working parameters of an ORC by using numerical analyses optimization method. *Energy Convers. Manag.* **2022**, *271*, 116301. [CrossRef]
18. Lai, N.A.; Wendland, M.; Fischer, J. Working fluids for high-temperature organic Rankine cycles. *Energy* **2011**, *36*, 199–211. [CrossRef]
19. Bellos, E.; Tzivanidis, C. Investigation of a hybrid ORC driven by waste heat and solar energy. *Energy Convers. Manag.* **2018**, *156*, 427–439. [CrossRef]

20. Özahi, E.; Tozlu, A.; Abuşoğlu, A. Thermoeconomic multi-objective optimization of an organic Rankine cycle (ORC) adapted to an existing solid waste power plant. *Energy Convers. Manag.* **2018**, *168*, 308–319. [CrossRef]
21. Siddiqi, M.A.; Atakan, B. Alkanes as fluids in Rankine cycles in comparison to water, benzene and toluene. *Energy* **2012**, *45*, 256–263. [CrossRef]
22. Song, C.; Gu, M.; Miao, Z.; Liu, C.; Xu, J. Effect of fluid dryness and critical temperature on trans-critical organic Rankine cycle. *Energy* **2019**, *174*, 97–109. [CrossRef]
23. Zhai, H.; Shi, L.; An, Q. Influence of working fluid properties on system performance and screen evaluation indicators for geothermal ORC (organic Rankine cycle) system. *Energy* **2014**, *74*, 2–11. [CrossRef]
24. Zhou, Y.; Liu, J.; Penoncello, S.G.; Lemmon, E.W. An Equation of State for the Thermodynamic Properties of Cyclohexane. *J. Phys. Chem. Ref. Data* **2014**, *43*, 043105. [CrossRef]
25. Abbas, W.K.A.; Vrabec, J. Cascaded dual-loop organic Rankine cycle with alkanes and low global warming potential refrigerants as working fluids. *Energy Convers. Manag.* **2021**, *249*, 114843. [CrossRef]
26. Tupper, E. *Introduction to Navel Architecture*, 4th ed.; Elsevier Butterworth-Heinemann: Oxford, UK, 2004.
27. Srinivasan, K.K.; Mago, P.J.; Krishnan, S.R. Analysis of exhaust waste heat recovery from a dual fuel low temperature combustion engine using an Organic Rankine Cycle. *Energy* **2010**, *35*, 2387–2399. [CrossRef]
28. Song, J.; Gu, C.-w. Performance analysis of a dual-loop organic Rankine cycle (ORC) system with wet steam expansion for engine waste heat recovery. *Appl. Energy* **2015**, *156*, 280–289. [CrossRef]
29. de la Fuente, S.S.; Greig, A.R. Making Shipping Greener: ORC Modelling in Challenging Environments. Available online: http://asme-orc2013.fyper.com/uploads/File/PPT%20092.pdf (accessed on 7 November 2013).
30. IMO 2022 Guidelines on the Method of Calculation of the Attained Energy Efficiency Existing Ship Index (EEXI). Available online: https://www.imo.org/ (accessed on 10 June 2022).
31. Song, J.; Gu, C.-w. Parametric analysis of a dual loop Organic Rankine Cycle (ORC) system for engine waste heat recovery. *Energy Convers. Manag.* **2015**, *105*, 995–1005. [CrossRef]
32. Usman, M.; Imran, M.; Lee, D.H.; Park, B.-S. Experimental investigation of off-grid organic Rankine cycle control system adapting sliding pressure strategy under proportional integral with feed-forward and compensator. *Appl. Therm. Eng.* **2017**, *110*, 1153–1163. [CrossRef]